Available online at www.sciencedirect.com
ScienceDirect
Int. J. Electron. Commun. (AEÜ) 63 (2009) 72–77
International Journal AEÜ of Electronics and Communications
www.elsevier.de/aeue

LETTER

Complex frequency shifted-perfectly matched layer for the finite-element time-domain method

Masoud Movahhedi[a,*], Abdolali Abdipour[b]

[a]*Department of Electrical Engineering, Shahid Bahonar University of Kerman, Kerman, Iran*
[b]*Department of Electrical Engineering, Amirkabir University of Technology (Tehran Polytechnic), Tehran, Iran*

Received 6 June 2007; accepted 3 October 2007

Abstract

We present a new formulation to implement the complex frequency shifted-perfectly matched layer (CFS-PML) for boundary truncation in three-dimensional vector finite-element time-domain method applied to the vector wave equation. It is shown that the proposed method is highly absorptive to evanescent modes, when computing the wave interaction of elongated structures or sharp corners, and can improve the performance of the boundary truncation, significantly. The impact of the CFS-PML parameters on the reflection error is investigated and optimal choices of these parameters are derived.

Keywords: Complex frequency shifted-perfectly matched layer (CFS-PML); Finite-element time-domain method; Vector wave equation

1. Introduction

The perfectly matched layer (PML) is very efficient and popular for grid truncation of open-region problems. Bérenger [1] introduced the PML in the context of the finite-difference time-domain (FDTD) scheme [2]. Bérenger used a decomposition of the fields in Maxwell's equations to derive a lossy medium which allows reflectionless transmission of an incident plane wave from an arbitrary angle of incidence. Chew and Weedon interpreted the PML as a complex coordinate stretching [3]. Later, it was shown in [4] that the non-physical field-splitting could be avoided and the PML be derived from Maxwell's equations in anisotropic media, which is called the unsplit or uniaxial (U)PML. In [5] a modification of the frequency-dependent attenuation function in [4] was introduced in the context of providing causality. The resulting PML has later been labeled the complex-frequency shifted (CFS)-PML. In the standard PML the numerical results were showing a late-time linear growth. The CFS-PML has been shown to remedy this problem and further the attenuation of evanescent waves is improved [6]. Expect the original form of Bérenger's PML [1], none of the above variants require field-splitting. Hence, they are more suitable for finite-element applications because they only detail the insertion of new constitutive tensors inside the PML region while keeping the basic form of the Maxwell equations invariant.

In the context of the finite-element method (FEM), the PML had been widely used for frequency-domain computations. The FEM is suitable for problems with complex geometry and/or rapidly varying field solutions. Time-domain formulations of the PML are attractive since one computation provides the response of an electromagnetic device in a broad frequency band and, more importantly, they are capable of simulation of nonlinear devices and media. However, the finite-element time-domain (FETD) formulation of the PML has been less investigated, which potentially limits the applicability of the FETD method for open region problems. Recently, a PML scheme to truncate FETD

* Corresponding author. Fax: +98 21 6640 6469.
E-mail addresses: movahhedi@ieee.org (M. Movahhedi), abdipour@aut.ac.ir (A. Abdipour).

1434-8411/$ - see front matter © 2007 Elsevier GmbH. All rights reserved.
doi:10.1016/j.aeue.2007.10.001

meshes for analyzing two-dimensional [7] and generally for three-dimensional [8,9] open-region electromagnetic problems have been developed. In [7], an implementation of the two-dimensional field-splitting formulation of the PML has been presented and in [8] and [9], the UPML formulation has been implemented and investigated for three-dimensional electromagnetic problems. We have developed, in a most recent paper [10], a new formulation for the FETD method augmented with the CFS-PML and applied it to two-dimensional radiating problems. In [10], the CFS-PML implementation for the FETD method which is applied directly to the Maxwell equations has been introduced; whereas all of the previous published papers have implemented the UPML for the FETD solution of the vector wave equation.

In this paper, we introduce the CFS-PML implementation for the FETD method applied to the second-order wave equation; whereas all of the previous published papers have implemented the UPML for the FETD solution of this equation. Using the CFS-PML formulation, instead of conventional UPML, will improve attenuation of evanescent waves in the simulated structure. The effectiveness of the proposed method is studied as a function of the constitutive parameters of the CFS-PML. Furthermore, the optimized parameters are extracted for FETD method. A numerical example is considered to show the lower reflection errors obtained by our implementation compared to the conventional PML implementation for FETD method.

2. Numerical formulation

The time-harmonic Maxwell's curl equations in an anisotropic PML absorbing media can be written in their most general form as

$$\nabla \times \tilde{\mathbf{E}} = -jw\mu\tilde{\tilde{\Lambda}}(w)\tilde{\mathbf{H}},$$
$$\nabla \times \tilde{\mathbf{H}} = jw\varepsilon\tilde{\tilde{\Lambda}}(w)\tilde{\mathbf{E}} + \tilde{\mathbf{J}}, \tag{1}$$

where $\tilde{\mathbf{E}} = \tilde{E}_x\hat{\mathbf{x}} + \tilde{E}_y\hat{\mathbf{y}} + \tilde{E}_z\hat{\mathbf{z}}$ is the electric field and $\tilde{\mathbf{H}} = \tilde{H}_x\hat{\mathbf{x}} + \tilde{H}_y\hat{\mathbf{y}} + \tilde{H}_z\hat{\mathbf{z}}$ is the magnetic field in the frequency domain. $\tilde{\tilde{\Lambda}}(w)$ is a tensor given in Cartesian coordinate by

$$\tilde{\tilde{\Lambda}}(w) = \begin{bmatrix} \dfrac{\tilde{S}_y(w)\tilde{S}_z(w)}{\tilde{S}_x(w)} & & \\ & \dfrac{\tilde{S}_x(w)\tilde{S}_z(w)}{\tilde{S}_y(w)} & \\ & & \dfrac{\tilde{S}_x(w)\tilde{S}_y(w)}{\tilde{S}_z(w)} \end{bmatrix}, \tag{2}$$

where

$$\tilde{S}_i(w) = 1 + \frac{\sigma_i}{jw\varepsilon_0}, \quad i = x, y, z \tag{3}$$

are the stretched-coordinate metrics, in which $\sigma_i \geqslant 0$ is the conductivity profile different from zero only in the PML region to provide attenuation for propagating waves. Kuzuoglu and Mittra showed in [5] that this metric would suffer from a poor absorption at low frequencies. They proposed a different one, named CFS-PML, where $\tilde{S}_i(w)$ is substituted by

$$\tilde{S}_i(w) = \kappa_i + \frac{\sigma_i}{\alpha_i + jw\varepsilon_0}. \tag{4}$$

Here, $\alpha_i > 0$ and $\kappa_i > 1$ are introduced to better absorb the evanescent waves with $\alpha_i = 0$ and $\kappa_i = 1$ outside the PML region. In the CFS-PML the κ_i parameter is very important and must be chosen carefully, but α_i is very small and can be neglected. Therefore, in the following, for simplicity of the formulations, we assume that $\alpha_i = 0$.

By eliminating the $\tilde{\mathbf{H}}$ from (1), and assuming the ε, κ_i and σ_i are constant within each element and $\alpha_i = 0$, we obtain the second-order vector wave equation

$$\nabla \times (\mu^{-1}\tilde{\tilde{\Lambda}}^{-1}\nabla \times \tilde{\mathbf{E}}) - w^2\varepsilon\tilde{\tilde{\Lambda}}\tilde{\mathbf{E}} = -jw\tilde{\mathbf{J}}, \tag{5}$$

where

$$\tilde{\tilde{\Lambda}}^{-1} = \left(\frac{\tilde{S}_x}{\tilde{S}_y\tilde{S}_z}\right)\hat{\mathbf{x}}\hat{\mathbf{x}} + \left(\frac{\tilde{S}_y}{\tilde{S}_x\tilde{S}_z}\right)\hat{\mathbf{y}}\hat{\mathbf{y}} + \left(\frac{\tilde{S}_z}{\tilde{S}_x\tilde{S}_z}\right)\hat{\mathbf{z}}\hat{\mathbf{z}}. \tag{6}$$

Transformation of (5) to the time domain using the convention $-w^2 \to \partial^2/\partial t^2$ and $jw \to \partial/\partial t$ leads to the equation

$$\varepsilon\overline{\Lambda}(t)\star\partial_t^2\mathbf{E} + \nabla \times (\mu^{-1}\overline{\Lambda}^{-1}(t)\star\nabla \times \mathbf{E}) + \partial_t\mathbf{J} = 0. \tag{7}$$

To seek the finite-element time-domain solution of (7), Galerkin's method is employed to convert this equation into the matrix equation. The weak-form solution, by using the perfectly electric conducting wall to terminate the PML, satisfies

$$\int\int\int_\Omega \{\varepsilon\mathbf{W}_i \cdot (\overline{\Lambda}(t)\star\partial_t^2\mathbf{E}) \nabla \times \mathbf{W}_i \cdot (\mu^{-1}\overline{\Lambda}^{-1}(t)\star\nabla \times \mathbf{E}) + \mathbf{W}_i \cdot \partial_t\mathbf{J}\}\,\mathrm{d}V = 0, \tag{8}$$

where $\mathbf{W}_i$ denotes the vector basis function. In order to obtain the finite element solution, the examined three-dimensional domain, Ω, in the xyz-volume is assumed to be discretized by a finite element mesh composed by N_t tetrahedral elements with N_e edges. In each point $\mathbf{r}$ of the simulation domain, Ω, the electric field $\mathbf{E}$ is approximated by the edge elements as

$$\mathbf{E}(\mathbf{r}, t) = \sum_{j=1}^{N} e_j(t)\mathbf{W}_j(\mathbf{r}), \tag{9}$$

where $e_j(t)$ is the electric field circulation along the ith edge, N denoting the total number of expansion functions and $\mathbf{W}_j(\mathbf{r})$ is the Whitney 1-form vector basis function associated to the ith edge [11] such that

$$\mathbf{W} \in \mathscr{H}(\mathrm{curl}; \Omega) = \{\mathbf{u} : \nabla \times \mathbf{u} \in [\mathscr{L}^2(\Omega)]^3\}. \tag{10}$$

The space $\mathscr{L}^2(\Omega)$ is the space of all functions on domain Ω that are square-integrable, which is often referred to as the space of functions with finite energy.

For Whitney 1-forms, the basis functions are well known by now. For example, for the edge ed{mn} where m and n are nodes of the edge, it is

$$\mathbf{W} = \xi_m \nabla \xi_n + \xi_n \nabla \xi_m, \tag{11}$$

where ξ_m is the Lagrange interpolation polynomial at vertex m [11].

By substituting (9) into (8) and assuming constant conductivities, σ_i, and κ_i within each element, the following ordinary differential equation is derived:

$$\sum_{e=1}^{M}\left(\mathbf{A}_1^e\frac{\mathrm{d}^2 e}{\mathrm{d}t^2}+\mathbf{A}_2^e\frac{\mathrm{d}e}{\mathrm{d}t}+\mathbf{A}_3^e e+\mathbf{B}_1^e e - \sum_{\xi=x,y,z}\mathbf{A}_\xi^e\psi_\xi-\sum_{\xi=x,y,z}\mathbf{B}_\xi^e\psi_\xi+f^e\right)=0. \tag{12}$$

Here, M denotes the total number of finite elements, $\mathbf{A}_1^e$, $\mathbf{A}_2^e$, $\mathbf{A}_3^e$, $\mathbf{B}_1^e$, $\mathbf{A}_\xi^e$, and $\mathbf{B}_\xi^e$ ($\xi = x, y, z$) are square matrices whose elements are given by

$$\begin{aligned}
&\mathbf{A}_1^e = \varepsilon\langle \mathbf{W}_i, \overline{T}_1.\mathbf{W}_j\rangle_{\Omega^e}, \quad \mathbf{A}_2^e = \varepsilon\langle \mathbf{W}_i, \overline{T}_2.\mathbf{W}_j\rangle_{\Omega^e}\\
&\mathbf{A}_3^e=\varepsilon\langle \mathbf{W}_i, \overline{T}_3.\mathbf{W}_j\rangle_{\Omega^e}, \quad \mathbf{A}_\xi^e=\varepsilon\langle \mathbf{W}_i, \overline{T}_\xi.\mathbf{W}_j\rangle_{\Omega^e}\ \ \xi=x, y, z\\
&\mathbf{B}_1^e = \mu^{-1}\langle \nabla\times\mathbf{W}_i, \overline{P}_1.\nabla\times\mathbf{W}_j\rangle_{\Omega^e}\\
&\mathbf{B}_\xi^e = \mu^{-1}\langle \nabla\times\mathbf{W}_i, \overline{P}_\xi.\nabla\times\mathbf{W}_j\rangle_{\Omega^e} \quad \xi = x, y, z,
\end{aligned} \tag{13}$$

where $\langle\cdot,\cdot\rangle_{\Omega^e}$ denotes the volume integration over element e, and $\overline{T}_1$, $\overline{T}_2$, $\overline{T}_3$, $\overline{T}_\xi$, $\overline{P}_1$, $\overline{P}_\xi$ are diagonal tensors given by

$$\begin{aligned}
\overline{T}_1 &= \left(\frac{\kappa_y\kappa_z}{\kappa_x}\right)\widehat{\mathbf{xx}}+\left(\frac{\kappa_x\kappa_z}{\kappa_y}\right)\widehat{\mathbf{yy}}+\left(\frac{\kappa_x\kappa_y}{\kappa_z}\right)\widehat{\mathbf{zz}},\\
\overline{T}_2 &= \varepsilon^{-1}[(\kappa_x^{-2}(\kappa_x\kappa_z\sigma_y+\kappa_y\kappa_x\sigma_z-\kappa_y\kappa_z\sigma_x))\widehat{\mathbf{xx}}\\
&\quad+(\kappa_y^{-2}(\kappa_y\kappa_z\sigma_x+\kappa_y\kappa_x\sigma_z-\kappa_z\kappa_x\sigma_y))\widehat{\mathbf{yy}}\\
&\quad+(\kappa_z^{-2}(\kappa_y\kappa_z\sigma_x+\kappa_x\kappa_z\sigma_y-\kappa_x\kappa_y\sigma_z))\widehat{\mathbf{zz}}],\\
\overline{T}_3 &= \varepsilon^{-2}[(\kappa_x^{-3}(\kappa_y\kappa_z\sigma_x^2-\kappa_x\sigma_x(\kappa_z\sigma_y+\kappa_y\sigma_z)+\kappa_x^2\sigma_y\sigma_z))\widehat{\mathbf{xx}}\\
&\quad+(\kappa_y^{-3}(\kappa_x\kappa_z\sigma_y^2-\kappa_y\sigma_y(\kappa_z\sigma_x+\kappa_x\sigma_z)+\kappa_y^2\sigma_x\sigma_z))\widehat{\mathbf{yy}},\\
&\quad+(\kappa_z^{-3}(\kappa_x\kappa_y\sigma_z^2-\kappa_z\sigma_z(\kappa_x\sigma_y+\kappa_y\sigma_x)+\kappa_z^2\sigma_y\sigma_x))\widehat{\mathbf{zz}}],\\
\overline{T}_x &= \varepsilon^{-2}[(\kappa_x^{-3}(\kappa_y\kappa_z\sigma_x^2-\kappa_x\sigma_x(\kappa_z\sigma_y+\kappa_y\sigma_z)+\kappa_x^2\sigma_y\sigma_z))\widehat{\mathbf{xx}}],\\
\overline{T}_y &= \varepsilon^{-2}[(\kappa_y^{-3}(\kappa_x\kappa_z\sigma_y^2-\kappa_y\sigma_y(\kappa_z\sigma_x+\kappa_x\sigma_z)+\kappa_y^2\sigma_x\sigma_z))\widehat{\mathbf{yy}}],\\
\overline{T}_z &= \varepsilon^{-2}[(\kappa_z^{-3}(\kappa_x\kappa_y\sigma_z^2-\kappa_z\sigma_z(\kappa_x\sigma_y+\kappa_y\sigma_x)+\kappa_z^2\sigma_y\sigma_x))\widehat{\mathbf{zz}}],\\
\overline{P}_1 &= \left(\frac{\kappa_x}{\kappa_y\kappa_z}\right)\widehat{\mathbf{xx}}+\left(\frac{\kappa_y}{\kappa_x\kappa_z}\right)\widehat{\mathbf{yy}}+\left(\frac{\kappa_z}{\kappa_y\kappa_x}\right)\widehat{\mathbf{zz}},\\
\overline{P}_x &= \left(\frac{1}{\kappa_x}\frac{\sigma_y\kappa_x-\sigma_x\kappa_y}{\sigma_z\kappa_x-\sigma_x\kappa_z}\right)\widehat{\mathbf{yy}}+\left(\frac{1}{\kappa_x}\frac{\sigma_z\kappa_x-\sigma_x\kappa_z}{\sigma_y\kappa_x-\sigma_x\kappa_y}\right)\widehat{\mathbf{zz}},\\
\overline{P}_y &= \left(\frac{1}{\kappa_y}\frac{\sigma_x\kappa_y-\sigma_y\kappa_x}{\sigma_z\kappa_y-\sigma_y\kappa_z}\right)\widehat{\mathbf{xx}}+\left(\frac{1}{\kappa_y}\frac{\sigma_z\kappa_y-\sigma_y\kappa_z}{\sigma_x\kappa_y-\sigma_y\kappa_x}\right)\widehat{\mathbf{zz}},\\
\overline{P}_z &= \left(\frac{1}{\kappa_z}\frac{\sigma_x\kappa_z-\sigma_z\kappa_x}{\sigma_y\kappa_z-\sigma_z\kappa_y}\right)\widehat{\mathbf{xx}}+\left(\frac{1}{\kappa_z}\frac{\sigma_y\kappa_z-\sigma_z\kappa_y}{\sigma_x\kappa_z-\sigma_z\kappa_x}\right)\widehat{\mathbf{yy}}.
\end{aligned} \tag{14}$$

In (12), $e = [e_1, e_2, ..., e_N]^{\mathrm{T}}$ is the unknown vector, f^e is the excitation vector given by

$$f^e = \langle \mathbf{W}_i, \partial_t \mathbf{J}(t)\rangle_{\Omega^e} \tag{15}$$

and ψ_ξ ($\xi = x, y, z$) are vectors whose elements can be expressed as

$$\psi_{\xi,i}(t) = \frac{\sigma_\xi}{\varepsilon\kappa_\xi}\mathrm{e}^{-(\sigma_\xi/\varepsilon_0\kappa_\xi)t}\overline{u}(t)\star e_i(t), \quad \xi = x, y, z \tag{16}$$

in which $\overline{u}(t)$ denotes the unit step function. The above convolution can be recursively evaluated as [12]

$$\psi_\xi^n = \mathrm{e}^{-(\sigma_\xi/\varepsilon_0\kappa_\xi)\Delta t}\psi_\xi^{n-1} + \frac{1}{\kappa_\xi}(1.0-e^{-(\sigma_\xi/\varepsilon_0\kappa_\xi)\Delta t})e^n, \quad \xi = x, y, z. \tag{17}$$

In which the field is assumed to be constant within each time step. The global matrices can be obtained from local matrices, and the symbolic summation (12) is carried out easily.

3. Numerical results

The proposed CFS-PML implementation for the FETD solution of the wave equation is tested on the following two-dimensional example and optimized PML parameters are obtained. This example is designed to measure the reflection from the CFS-PML for approximately tangential incidence. Fig. 1 illustrates the simulated problem involving a current source **J** radiating *TE*-polarized waves in an elongated FETD grid. The excitation has the form of a modulated Gaussian pulse. The center frequency and bandwidth of the excitation current are 6×10^{11} Hz and 3.5×10^{11} Hz, respectively. The reflection error in the electric field is computed at points A, B, C, and D. A reference solution is obtained by setting the ends sufficiently far. The computational domain is discretized by uniform triangular elements with $\Delta x = \Delta y = 5.2\times10^{-2}$ mm. The PML region has a thickness of $d = 3.64\times10^{-1}$ mm and is terminated by a perfectly electric wall. The profiles of the PML parameters (σ and κ)

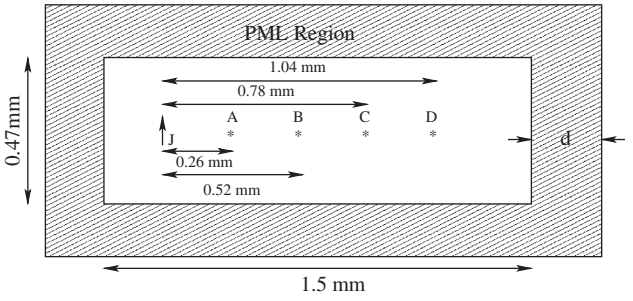

Fig. 1. Current element **J** radiating in an elongated FETD grid terminated by CFS-PML.

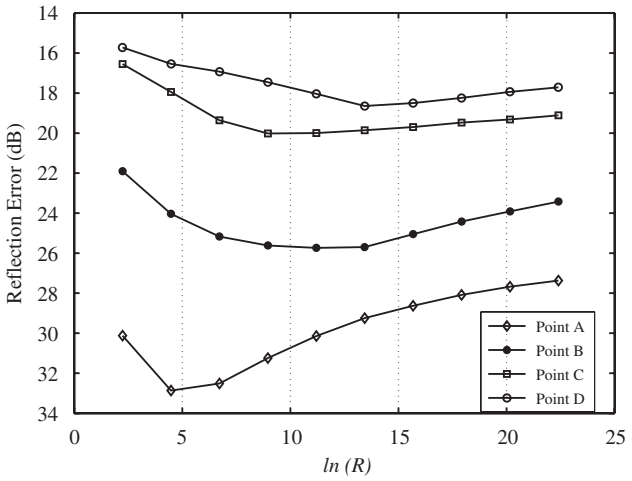

Fig. 2. Maximum reflection error at points A, B, C, and D due to a polynomial-scaled CFS-PML versus $-\ln(R)$. Parameters $\kappa = 1$ and $m = 4$.

are determined by the following:

$$\sigma = \sigma_{\max}\left(\frac{\rho}{d}\right)^m, \quad \sigma_{\max} = -\frac{(m+1)ln(R)}{2\eta d}$$
$$\kappa = 1 + (\kappa_{\max} - 1)\left(\frac{\rho}{d}\right)^m, \tag{18}$$

where ρ is the location of an element center, m is the profile order, η is the free space wave impedance, d is the physical depth of the PML region, and R is the theoretical reflection error at normal incidence.

The design of an effective PML region requires balancing the theoretical reflection error R and the numerical discretization error. In other words, the optimal values for m, $\sigma_{\max}$ and $\kappa_{\max}$ should be chosen. We have found that $3 \leqslant m \leqslant 4$ to be nearly optimal for this example and some other FETD simulations. To choose the optimal value for $\sigma_{\max}$ we need to determine R. Fig. 2 shows the maximum reflection error recorded at the observation points as a function of $-\ln(R)$ when $\kappa_{\max} = 1$. As it can be seen, with

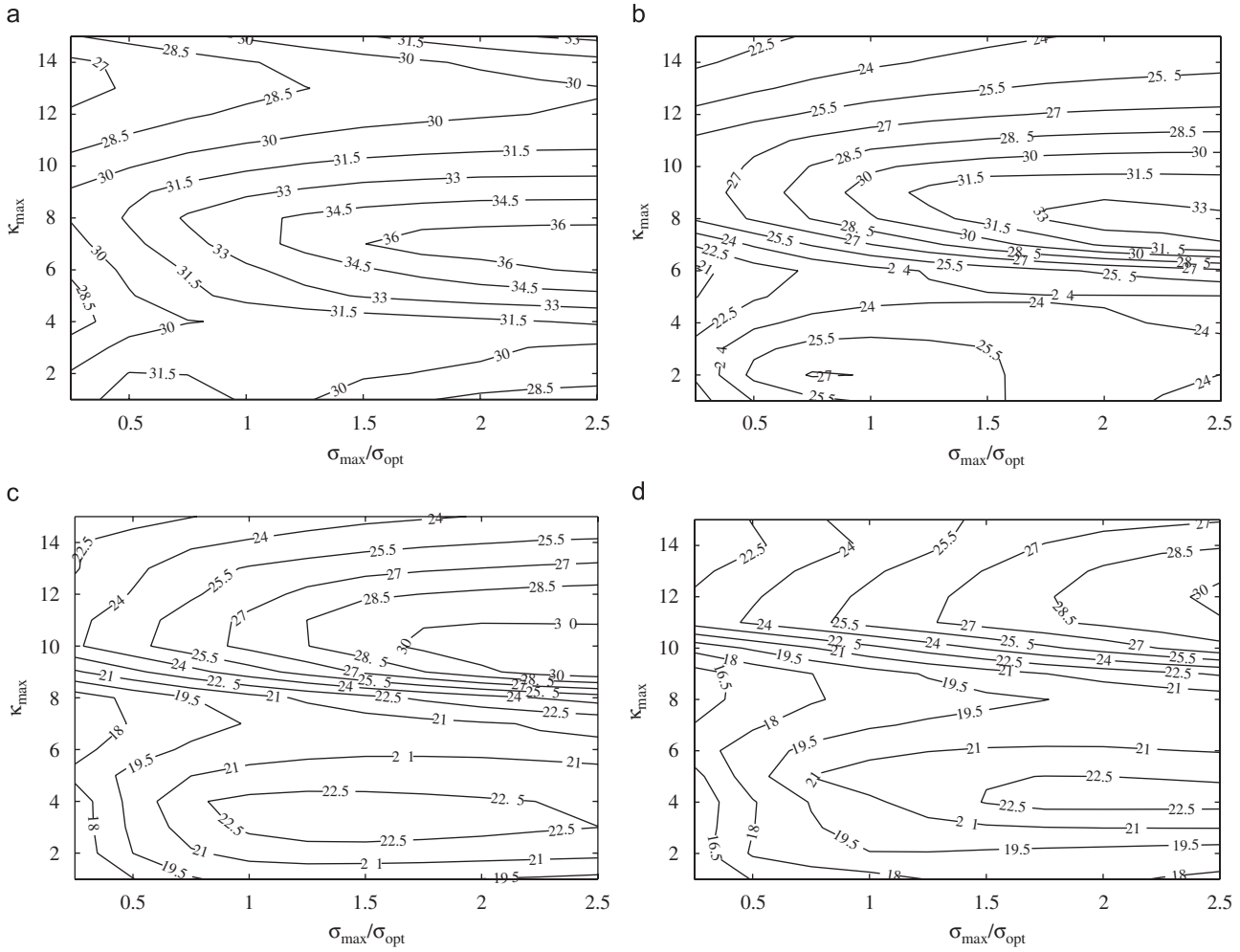

Fig. 3. Contour plots of the maximum reflection error in dB versus $\kappa_{\max}$ and $\sigma_{\max}/\sigma_{\text{opt}}$ for a polynomial-scaled CFS-PML at different points: (a) at point A, (b) at point B, (c) at point C, and (d) at point D.

decreasing the angle of incidence to the PML layer, the reflection error is greatly improved (reflection error at point A is more less than at point D). An average optimal choice for σ_{max} at different points, called σ_{opt}, can be reached when $R \simeq e^{-10}$.

We now note that the radiation due to the current source is characterized by a wide spectrum of waves containing evanescent as well as propagating modes. However, the evanescent modes are not absorbed by the PML when $\kappa = 1$. Increasing κ should help this situation. To investigate this possibility and observe the maximum reflection error as a function of the CFS-PML constitutive parameters, Fig. 3 illustrates the contour plots of the reflection error at different points versus $\sigma_{max}/\sigma_{opt}$ and κ_{max}. As expected, this figure shows that increasing κ_{max} leads to a decrease of the reflection error. For instance, it is demonstrated in Fig. 3(c) that at point C, the maximum reflection error is on the order of -30 dB (reached with $9 \leqslant \kappa_{max} \leqslant 11$ and $1.6\sigma_{opt} \leqslant \sigma_{max} \leqslant 3\sigma_{opt}$). For traditional PML with $\kappa = 1$, the maximum reflection error is on the order of -19 dB (Fig. 2). This is almost a 11 dB improvement over the traditional PML. As it is shown in Fig. 3, choosing σ_{max} in the range of $2\sigma_{opt} \leqslant \sigma_{max} \leqslant 2.7\sigma_{opt}$ leads to an optimal error for different angles of incidence to the PML layer. Due to the variation of the optimal value of κ_{max} at different points, the exact optimal value for κ_{max} cannot be determined. But with a good approximation, it can be chosen equal to $\kappa_{max} \cong 10$.

4. Conclusion

We have described a new CFS-PML implementation for the FETD solution of the second order wave equation. Moreover, the optimum choices of the CFS-PML constitutive parameters have been derived. These optimal values can be considered as $2\sigma_{opt} \leqslant \sigma_{max} \leqslant 2.7\sigma_{opt}$ and $\kappa_{max} \cong 10$. It was demonstrated that the CFS form of the stretched-coordinate variables enhances its ability to absorb evanescent waves. A maximum reflection error of about -30 dB was recorded for the example, compared to -19 dB for the PML formulation with $\kappa = 1$. This is almost a 11 dB improvement over the traditional PML.

References

[1] Bérenger J. A perfectly matched layer for the absorption of electromagnetic waves. J Comput Phys 1994;144:185–200.
[2] Yee KS. Numerical solution of initial boundary value problems involving Maxwell's equations in isotropic media. IEEE Trans Antennas Propag 1966;AP-14:302–7.
[3] Chew WC, Weedon W. A 3d perfectly matched medium from modified Maxwell's equations with stretched coordinates. Microwave Opt Tech Lett 1994;7:599–604.
[4] Sacks ZS, Kingsland DM, Lee R, Lee JF. A perfectly matched anisotropic absorber for use as an absorbing boundary condition. IEEE Trans Antennas Propag 1995;43:1460–3.
[5] Kuzuoglu M, Mittra R. Investigation of nonplanar perfectly matched absorbers for finite-element mesh truncation. IEEE Trans Antennas Propag 1997;45:474–86.
[6] Bérenger J. Application of the cfs-pml to the absorption of evanescent waves in waveguides. IEEE Microwave Wireless Comp Lett 2002;12:218–20.
[7] Jiao D, Jin J-M. An effective algorithm for implementing perfectly matched layers in time-domain finite-element simulation of open-region em problems. IEEE Trans Antennas Propag 2002;50:1615–23.
[8] Jiao D, Jin J-M, Michielssen E, Riley DJ. Time-domain finite-element simulation of three-dimensional scattering and radiation problems using perfectly matched layers. IEEE Trans Antennas Propag 2003;51:296–305.
[9] Rylander T, Jin J-M. Perfectly matched layer in three dimensions for the time-domain finite element method applied to radiation problems. IEEE Trans Antennas Propag 2005;53:1489–99.
[10] Movahhedi M, Abdipour A, Ceric H, Sheikholeslami A, Selberherr S. Optimization of the perfectly matched layer for the finite-element time-domain method. IEEE Microwave and Wireless Components Lett 2007;17:10–2.
[11] Bossavit A. Whitney forms: a class of finite elements for three-dimensional computations in electromagnetism. IEE Proc 1988;135:493–500.
[12] Roden J, Gedney SD. Convolution pml: An efficient fdtd implementation of the cfs-pml for arbitrary media. Microwave Opt Tech Lett 2000;27:334–9.

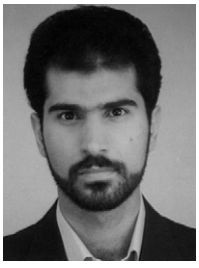

Masoud Movahhedi was born in Yazd, Iran, in 1976. He received the B.Sc. degree from Sharif University of Technology, Tehran, Iran, in 1998, the M.Sc. and Ph.D. degrees from Amirkabir University of Technology (Tehran Polytechnic), Tehran, Iran, in 2000 and 2007, all in electrical engineering.
From December 2005 to September 2006, he was with the Institute for Microelectronics, Technische Universität Wien, Austria, as a Visiting Student. He is currently an Assistant Professor with the Electrical Engineering Department, Shahid Bahaonar University of Kerman, Kerman, Iran. His research interests are in the areas of computer-aided design of microwave integrated circuits, computational electromagnetic, semiconductor high-frequency RF modeling, and interconnect simulations.
Dr. Movahhedi was the recipient of the GAAS-05 Fellowship sponsored by the GAAS Association to young graduate researchers for his paper presented at GAAS2005. He was also the recipient of the Electrical Engineering Department Outstanding Student Award in 2005 and 2006.

Abdolali Abdipour was born in Alashtar, Iran, in 1966. He received the B.Sc. degree in electrical engineering from Tehran University, Tehran, Iran, in 1989, the M.Sc. degree in electronics from Limoges University, Limoges, France, in 1992, and the Ph.D. degree in electronic engineering from Paris XI university, Paris, France, in 1996.

He is currently a Professor with the Electrical Engineering Department, Amirkabir University of Technology (Tehran Polytechnic), Tehran, Iran. He authored two books, *Noise in Electronic Communication: Modeling, Analysis and measurement* (AmirKabir Univ. Press, 2005, in Persian) and *Transmission Lines* (Nahre Danesh Press, 2006, in Persian). His research areas include wireless communication systems (RF technology and transceivers), RF/microwave/millimeter-wave circuit and system design, electromagnetic (EM) modeling of active devices and circuits, high-frequency electronics (signal and noise), nonlinear modeling, and analysis of microwave devices and circuits. He has authored or coauthored over 115 papers in refereed journals and local and international conferences.

Currently, he is Head of Electrical Engineering Department, Amirkabir University of Technology (Tehran Polytechnic) and also Director of Radio Communication Center of Excellence.